RSC Advances

PAPER

View Article Online
View Journal | View Issue

Cite this: *RSC Adv.*, 2022, **12**, 1177

Facile synthesis of $Ni(OH)_2$ nanoarrays on graphene@carbon fabric as dual-functional electrochemical materials for supercapacitors and capacitive desalination†

Xin Liu,[a] Shi Du,[a] Xiaofan Zuo,[a] Xin Zhang *[bc] and Yu Jiang[d]

A high-performance $Ni(OH)_2$ nanoarray on graphene (RGO)@carbon fabric nanocomposites with hierarchical nanostructures were facilely synthesized, which involves (i) coating of graphene on a carbon fabric; and (ii) *in situ* growth of $Ni(OH)_2$ nanoarray on the graphene surface. It was found that $Ni(OH)_2$ nanoplates grew evenly on the surface of graphene without stacking. This unique structure of the electrode material favors a higher electrochemical active site, endowing the enhancing capacity performance. The morphology and microstructure of the as-prepared composites were characterized by X-ray diffraction (XRD), transmission electron microscopy (TEM), and scanning electron microscopy (SEM) techniques. Capacitive properties of the as-synthesized electrodes were studied *via* cyclic voltammetry, charge/discharge, and electrochemical impedance spectroscopy in a three-electrode experimental setup. Taking advantage of the unique structure of $Ni(OH)_2$/RGO@carbon fabric nanocomposites, this material as dual-functional electrodes shows decent performance for both supercapacitors and capacitive desalination (CDI). The specific capacitance was calculated to be 1325 F g^{-1} at 1 A g^{-1}; moreover, this material shows a high rate capability, whereby the capacitance can be maintained at 612 F g^{-1} even at 10 A g^{-1}. Besides, its performance as potential CDI electrodes was explored. Such high-performance $Ni(OH)_2$/RGO@carbon fabric hierarchical nanostructures can offer great promise in large-scale energy storage device applications.

Received 15th October 2021
Accepted 3rd December 2021

DOI: 10.1039/d1ra07633g

rsc.li/rsc-advances

1. Introduction

The utilization of environmentally friendly energy resources urges the development of energy storage devices with large capacitance, high density and long life. Supercapacitors, as promising candidates for energy storage devices, have unique characters, such as high power density, long cycle life, and small size, enabling them to be used as backup power sources in portable electronic devices, pacemakers, and hybrid electric vehicles.[1–5] The high performance of the supercapacitors is highly dependent on the rational design of novel electrode materials, which requires maximizing the electrochemically active sites of the electrodes, and this will benefit in facilitating more efficient charge and mass transportations.[6] According to the charge storage mechanism, supercapacitors can be divided into two basic classes: electric double layer capacitance (EDLC) and pseudocapacitance. Carbon-based materials are regarded as typical EDLC supercapacitors as their capacitance depends mainly on the specific area, and they always possess long cycle life and good mechanical properties.[7] Meanwhile, metal oxides/hydroxides (such as RuO_2, MnO_2, Co_3O_4, $Ni(OH)_2$ and layered double hydroxides (LDHs)) and conducting polymers (such as polyaniline, polypyrrole and polythiophene) are usually considered as pseudocapacitive active species.[8–20] These materials can deliver relatively high capacitance, which comes from the redox process of the electrodes; however, their poor stability because of structural degradation always hinders their practical application.[21–23] Therefore, efforts have been made to overcome these drawbacks.

In recent years, graphene-based electrodes have received increasing interest because of their excellent electrochemical stability, good structural, electrical and mechanical properties.[23] These studies mainly focus on the synthesis of binder-free, free-standing and flexible electrodes by assembling graphene (RGO) sheets into macroscopic RGO-based papers or films.[24–26] However, the effective surface area of graphene

[a]*Department of Environmental Engineering, College of Biology and the Environment, Nanjing Forestry University, Nanjing 210037, P. R. China*
[b]*College of Resources and Environment, University of Chinese Academy of Sciences, Beijing 101408, China. E-mail: xzhang@ucas.ac.cn; Tel: +86-10-69672964*
[c]*Yanshan Earth Critical Zone and Surface Fluxes Research Station, University of Chinese Academy of Sciences, Beijing 101408, China*
[d]*Jiangsu Provincial Ecological Assessment Center (Jiangsu Provincial Management Center for Emissions Registration and Exchange), Nanjing 210036, P. R. China*

† Electronic supplementary information (ESI) available. See DOI: 10.1039/d1ra07633g

materials is highly related to the layers, that is, fewer layered without agglomeration is expected to exhibit higher effective surface area. The irreversible agglomeration and restack of graphene nanosheets led to a lower specific surface area of graphene-based paper compared with exfoliated graphene nanosheets. Therefore, numerous methods were developed to enlarge the specific surface area of the pristine graphene. It is found that incorporating carbon materials with pseudocapacitive materials is helpful to relieve these problems. Among the pseudocapacitive materials, $Ni(OH)_2$ is one of the most promising candidates because of its low cost, environmental-benign nature and high pseudocapacitive activity. So, synthesis methods and morphologies of $Ni(OH)_2$ have been developed to improve the electrochemical properties.[27–31] For example, Shen *et al.* reported the synthesis discus-like $Ni(OH)_2$ hierarchical structure for supercapacitors,[29] and Li *et al.* prepared $Ni(OH)_2$ nanosheets as electrode materials for supercapacitors.[28] Among them, $Ni(OH)_2$ with an exploited structure and without any surfactant demonstrated to be highly effective for high-performance $Ni(OH)_2$ electrodes.

In the present study, we demonstrated a novel structure based on the graphene/$Ni(OH)_2$ nanostructured carbon fabric where solution exfoliated graphene nanosheets were first coated on carbon fibers, serving as conductive three-dimensional (3D) frameworks for the subsequent deposition of $Ni(OH)_2$ nanomaterials. Interestingly, a morphology transformation between the as-synthesis of $Ni(OH)_2$ flower and $Ni(OH)_2$ nanoarray decorated on graphene hierarchical nanostructured was observed, implying the exploitation of $Ni(OH)_2$ and in favor of improving the electrochemical surface area. These hierarchical 3D networks not only permitevenly exploited growth of graphene and $Ni(OH)_2$ but also facilitate the access between electrolytes and electrodes. Besides, this binder-free synthesis method will further improve the conductivity of the electrode. Furthermore, its performance as potential electrode materials has been less developed. These graphene/$Ni(OH)_2$ hierarchical nanostructures based on carbon fibers had improved capacitive performance compared to $Ni(OH)_2$ flowers.

2. Experimental

2.1. Preparation of $Ni(OH)_2$ nanoflower and graphene/$Ni(OH)_2$@carbon fiber hierarchical nanostructures

All the chemical reagents used in the experiments were obtained from commercial sources as guaranteed-grade reagents and used without further purification.

$Ni(OH)_2$ nanoflowers were synthesized by the hydrothermal method. In a typical synthesis, 0.27 g $Ni(NO_3)_2 \cdot 6H_2O$ was dissolved in a solvent mixture containing 25 mL of deionized water and 1 mL of ethylene glycol to form a transparent solution *via* magnetic stirring, and then 0.24 g of urea was added to the mixed solution. After stirring for about 0.5 h, the mixture was transferred to a Teflon-lined stainless steel autoclave and heated at 160 °C for 12 h in an oven. The solid product was then collected, washed with deionized water and ethanol several times, respectively, and then dried in an oven at 60 °C for 8 h.

The synthetic procedure of graphene/$Ni(OH)_2$@carbon fiber hierarchical nanostructures was as follows: (1) carbon fiber was ultrasonicated and soaked in a 1 M HNO_3 solution for 24 h, then washed with water and ethanol several times, followed by drying in an oven at 40 °C for 8 h, and finally recording the mass of the carbon fiber; (2) graphene oxide (GO) was prepared from natural graphite powder through a modified Hummers' method,[31] and the as-synthesis of graphene oxides (GO) was ultrasonicated for further use; (3) 10 mL of GO (1 mg mL^{-1}) solution was added to a mixture of 5 mL ethylene glycol and 10 mL deionized water, stirred for 2 h, and then transferred to a Teflon-lined stainless steel autoclave that was heated at 160 °C for 12 h. During this process, GO could be reduced to RGO, whereby the coat outside the carbon fibers were washed with water and ethanol, dried at 40 °C for 8 h, and the final mass was recorded (denoted as graphene@carbon fiber (RGO/CF)) (4) the graphene/$Ni(OH)_2$@carbon fiber was synthesized using a similar method as $Ni(OH)_2$ nanoflowers, except for the addition of the as-synthesized graphene@carbon fiber. The products were washed with water and ethanol, dried at 60 °C for 8 h, and the final mass recorded (graphene/$Ni(OH)_2$@carbon fiber (RGO/$Ni(OH)_2$@CF)). The total mass loading of graphene/$Ni(OH)_2$ on the copper foam substrate was about 2.3 mg.

2.2. Material characterizations

The X-ray Diffraction (XRD) patterns of samples were collected on a Rigaku D/max-2400 diffractometer, operated at 40 kV voltage and 200 mA current using Cu Kα radiation (l = 1.5418 Å). The morphologies were analyzed *via* Hitachi H-800 transmission electron microscopy (TEM) and scanning electron microscopy (SEM, Hitachi S-3000N) techniques.

2.3. Electrochemical measurements

All the electrochemical measurements were carried out in a conventional three-electrode system in a 6 M NaOH aqueous electrolyte at room temperature. The as-synthesized $Ni(OH)_2$/RGO@CF, a platinum wire electrode and a silver chloride electrode (Ag/AgCl) were used as the working electrode, counter electrode and reference electrode, respectively. The electrochemical performances of the as-prepared material electrodes were tested *via* cyclic voltammetry (CV), galvanostatic charge/discharge and electrochemical impedance spectroscopy (EIS) on an electrochemical workstation (CHI 660D, Shanghai CH Instrument Company, China). The measurements were carried out in a 6 M NaOH aqueous electrolyte at room temperature. CV tests were done between 0 V to 0.5 V (*vs.* Ag/AgCl) at scan rates of 2, 10, 20, 40, 50 and 100 mV s^{-1}. Galvanostatic charge/discharge curves were measured in the potential range of 0–0.4 V at different current densities, and the EIS measurements were carried out in the frequency range from 100 kHz to 0.5 Hz at open circuit potential with an ac perturbation of 5 mV.

2.4. Electrosorption experiment

The removal of NaCl was measured using a continuously recycling system that consists of a peristaltic pump, a CDI unit cell,

a power supply and a conductivity monitor. In the experiment, the NaCl concentration was fixed at 164.7 mg L^{-1} at various voltages ate a flow rate of 10 mL min^{-1} in 30 min at room temperature, and the conductivity was recorded.

In this experiment, the salt removal capacity (mg g^{-1}) was defined as below:

$$\Gamma = \frac{(C_0 - C_e)V}{m}$$

where C_0 and C_e (mg L^{-1}) is the initial and final concentrations of NaCl, V is the volume of NaCl (L), and m is the total mass of both electrodes (g).

3. Results and discussion

The formation of $Ni(OH)_2$/RGO@CF can be explained as follows (Scheme 1): first, GO was adsorbed on the treated carbon fibers. Then, *via* the hydrothermal method, the graphene/carbon fiber can be obtained, followed by the second step of growth of $Ni(OH)_2$ nanosheets on the graphene/carbon fiber. Powder XRD patterns of $Ni(OH)_2$ and RGO/$Ni(OH)_2$@CF nanocomposites are shown in Fig. 1. It is clearly seen that the diffraction peaks at 19.5°, 33.6°, 39.0°, 52.7°, 60.0°, 63.6°, 70.8° and 73.7° in the composites can be attributed to the characteristic reflections of (001), (100), (101), (102), (110), (111), (103) and (201) crystalline planes of $Ni(OH)_2$ (JCPDS no. 14-0117), respectively.[13] Moreover, for the XRD spectrum of $Ni(OH)_2$/RGO@CF nanocomposites, some of the peaks of $Ni(OH)_2$ are not as clear as those of pure $Ni(OH)_2$ because of the sharp peaks of carbon fibers. Also, diffraction peaks corresponding to graphene and carbon fibers (at ~25° and ~43°) were observed.

The morphologies of $Ni(OH)_2$, RGO@CF and RGO/$Ni(OH)_2$@CF nanocomposites were characterized by TEM and SEM measurements, as shown in Fig. S1† and 2. The TEM images of $Ni(OH)_2$ (Fig. S1†) indicate that this nanomaterial showed a uniform flower-like structure, which aggregated randomly by nanosheets with wrinkles, thus corresponding to the SEM images of $Ni(OH)_2$ in Fig. 2(a)–(c). Fig. 2(d)–(f) present the SEM images of RGO@CF with different magnified RGO coated on the surface of carbon fibers with the exfoliated transparent sheet structure. For $Ni(OH)_2$/RGO@CF hierarchal nanocomposites, the $Ni(OH)_2$ nanosheets that are different from the self-assembled pure $Ni(OH)_2$ nanoflowers, Fig. 2(g)–(i), decorated on the surface of RGO@CF without stacking (Fig. 2b). This structure endowed $Ni(OH)_2$/RGO@CF nanocomposites with a higher active electrochemical surface area.

The electrochemical performances of the obtained $Ni(OH)_2$ and $Ni(OH)_2$/RGO@CF nanocomposites were investigated in a three-electrode cell with 6 M NaOH by CV, charge/discharge and EIS measurements. Fig. 3(a) and (b) show the typical CV curves of $Ni(OH)_2$ and $Ni(OH)_2$/RGO@CF nanocomposites electrodes at various scan rates ranging from 2 mV s^{-1} to 100 mV s^{-1} between 0 to 0.5 V (*vs.* Ag/AgCl), respectively. It is seen that there exists a pair of redox peaks corresponding to the pseudocapacitive behavior of $Ni(OH)_2$. Also, it is apparent that the $Ni(OH)_2$/RGO@CF nanocomposites compared with the pure $Ni(OH)_2$ electrodes showed a higher integrated surface area due to the contribution of electric double-layer capacitance from graphene and pseudocapacitance capacitance from $Ni(OH)_2$. With the increasing scan rates, it is clear that the reduction and oxidation peaks exhibited a slight shift, corresponding to higher reversibility.

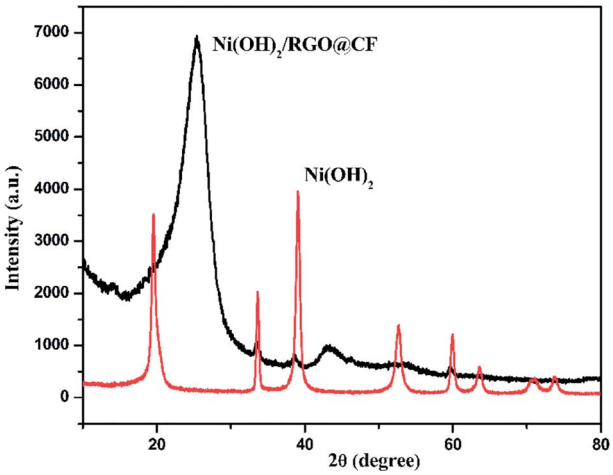

Fig. 1 XRD of CF/RGO $Ni(OH)_2$ and $Ni(OH)_2$/RGO@CF.

Fig. 4 further shows the galvanostatic charge–discharge (GCD) performance of $Ni(OH)_2$ and $Ni(OH)_2$/RGO@CF. The GCD tests were conducted in 6 M NaOH within a voltage range of 0–0.4 V at various current densities ranging from 1 to 10 A g^{-1}. The mass capacitance for a nonlinear discharge curve resulted from the pseudocapacitance of $Ni(OH)_2$, corresponding to the CV curves. The specific capacitances (C_s) of the electrodes can be calculated according to the following equation:

$$C_s = \frac{It}{(\Delta V)m}$$

where m (g) is the mass of the active material in the electrode, I (A) is the discharge current, ΔV (v) is the potential window, t is the discharge time, and C_s (F g^{-1}) is the specific capacitance. As shown in Fig. 4(a) and (b), the specific capacitance of $Ni(OH)_2$/RGO@CF nanocomposites were higher than $Ni(OH)_2$, which was in good agreement with the trend of CV curves. The specific capacitance of the $Ni(OH)_2$/RGO@CF composites was calculated to be 1325, 986, 862, 790, 753 and 612 F g^{-1} at 1 A g^{-1} to 10 A g^{-1} for the first cycle, respectively, which are higher than pristine $Ni(OH)_2$ at any current density (560, 498, 462, 434, 413 and 338 F g^{-1} at 1 A g^{-1} to 10 A g^{-1}). Also, the results are even higher than the former reported rGO/$Ni(OH)_2$/PANI 514 F g^{-1} at 2 A g^{-1} current density[34] and three

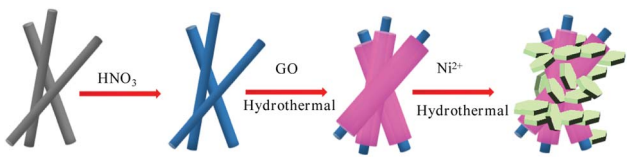

Scheme 1 The synthesis of $Ni(OH)_2$/RGO@CF.

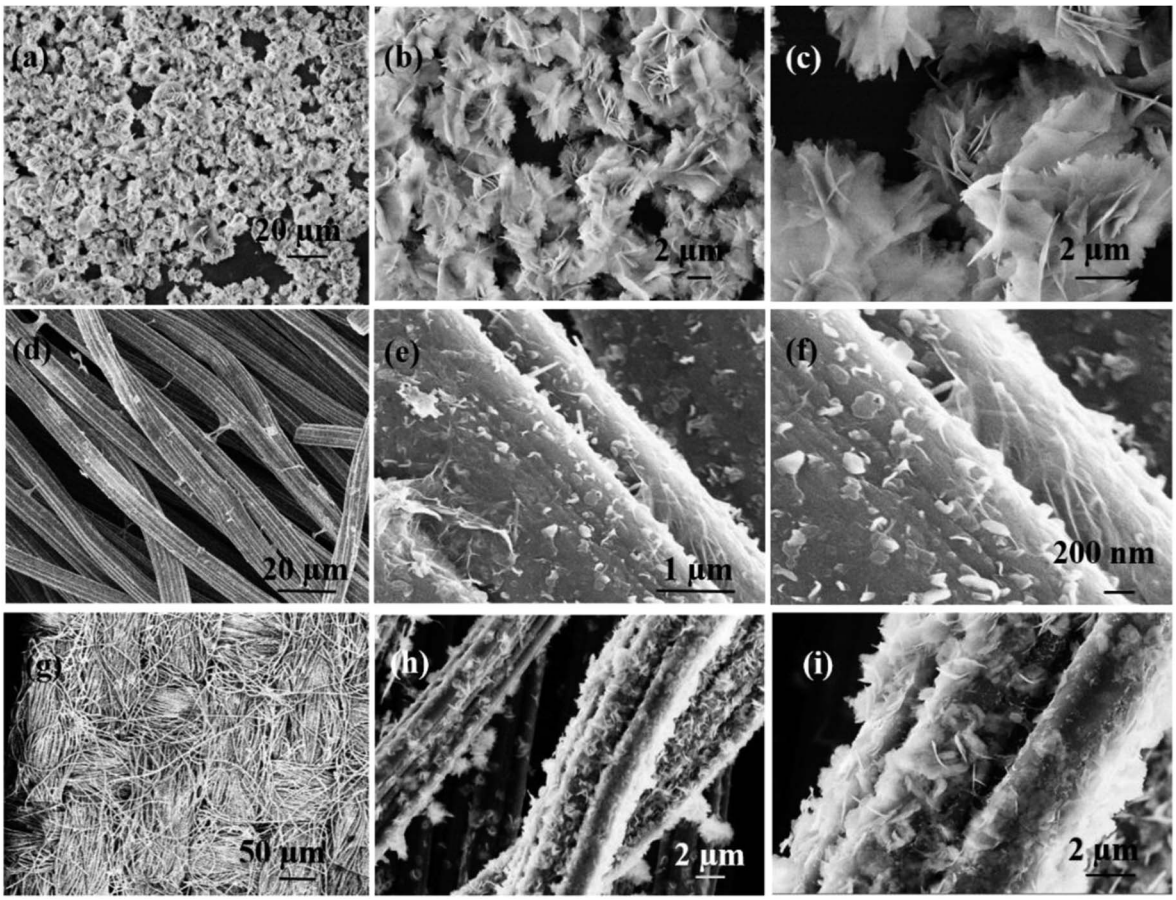

Fig. 2 The morphologies of $Ni(OH)_2$ nanoflowers (a–c) RGO@CF (d–f) and $Ni(OH)_2$/RGO@CF (g–i) with different magnifications.

dimensional $Ni(OH)_2$/rGO hydrogel with the highest capacitance of 532 F g^{-1}.[35]

This suggests that about 53.8% of the specific capacitance value at 1.0 A g^{-1} was maintained when the current density increased to 10 A g^{-1} for $Ni(OH)_2$/RGO@CF composites. The rate capability of these two electrodes was investigated, as shown in Fig. 4(c) and (d). For both electrodes, the capacitance was more stable from the current density of 2 A g^{-1}, which may be caused by impurities at the surface of the electrodes at the start of the experiments. However, they tend to be stable at the

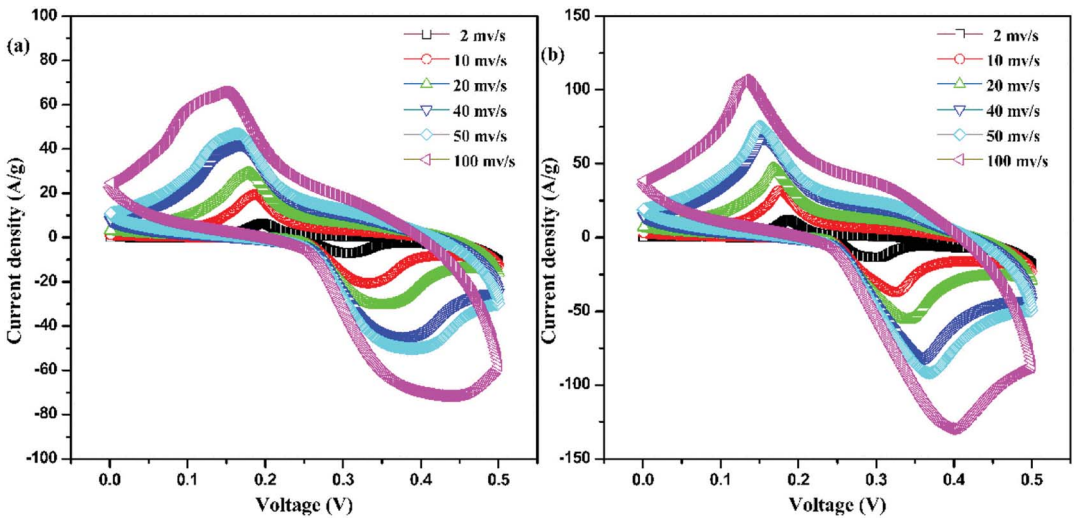

Fig. 3 The CV curves of $Ni(OH)_2$ (a) and $Ni(OH)_2$/RGO@CF (b) in 6 M NaOH at different scan rates.

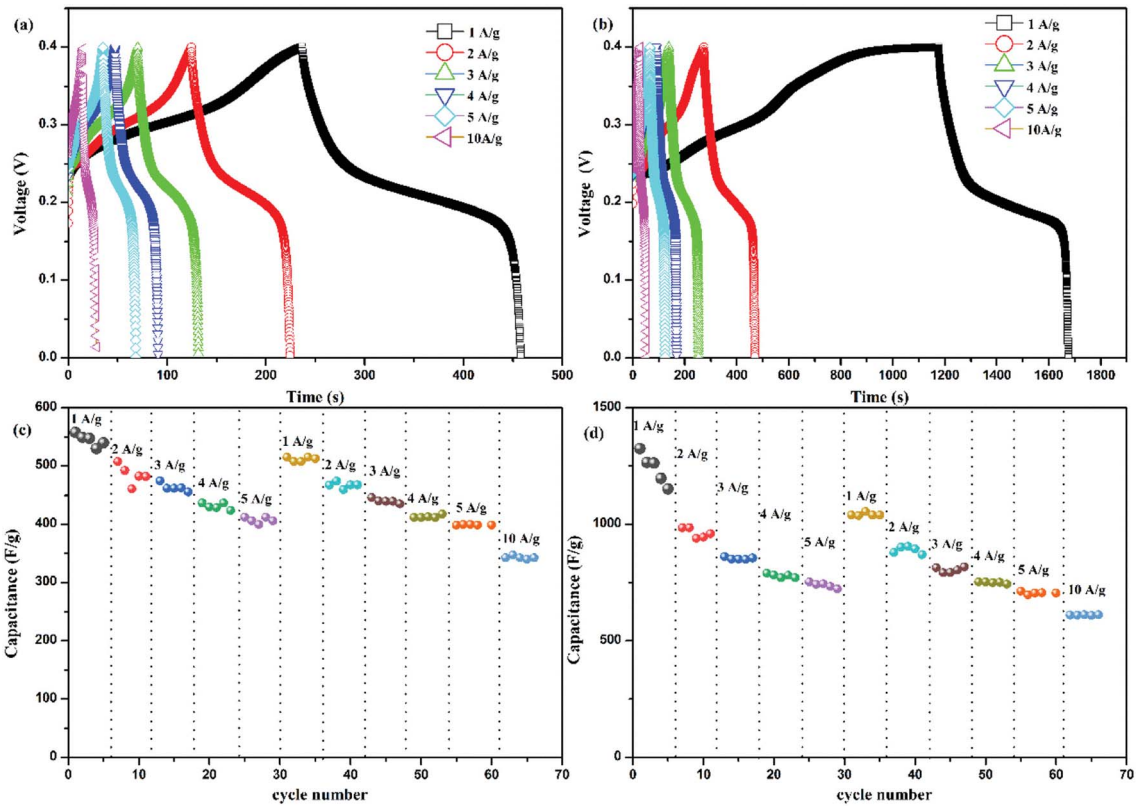

Fig. 4 Galvanostatic charge–discharge curves of $Ni(OH)_2$ (a) and $Ni(OH)_2$/RGO@CF (b); rate-capability test for $Ni(OH)_2$ (c) and $Ni(OH)_2$/RGO@CF at various current densities (1–10 A g^{-1}) (d).

second cycle from 1 to 10 A g^{-1}. Besides, at the same current density, they all showed a low decrease of the capacitance, which indicates good rate capability of the electrodes and the capacitance of $Ni(OH)_2$/RGO@CF was higher than $Ni(OH)_2$ at each current density. The enhancement of the $Ni(OH)_2$/RGO@CF capacitance can be attributed to the combination of the EDLC of RGO and the faradaic pseudocapacitance of $Ni(OH)_2$ nanosheets and the unique hierarchical structure of the electrodes.

Fig. 5(a) displays the Nyquist plots of $Ni(OH)_2$ and $Ni(OH)_2$/RGO@CF composite electrodes. The Nyquist plot spectrum can reflect the conductivity and the ion diffusion performance of electrodes. Usually, the Nyquist plot can be divided into three regions. In the high-frequency region, the intercept of the real axis indicates a combined resistance (R_s), which is produced by the bulk resistance of the electrodes, a contact resistance between the current collector/electroactive material and electrolyte. The semicircle relates to the charge transfer resistance

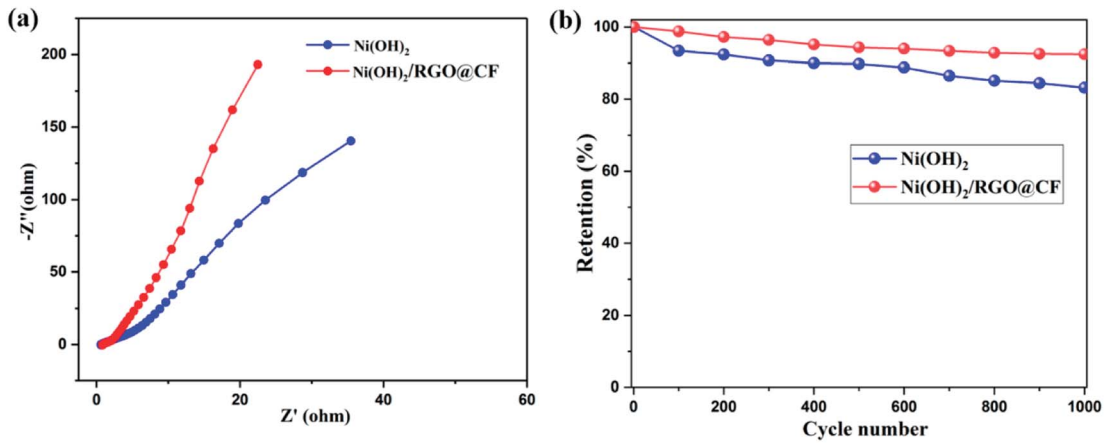

Fig. 5 (a) Nyquist plots of $Ni(OH)_2$ (a) and $Ni(OH)_2$/RGO@CF, (b) cyclic stability of $Ni(OH)_2$ (a) and $Ni(OH)_2$/RGO@CF electrodes.

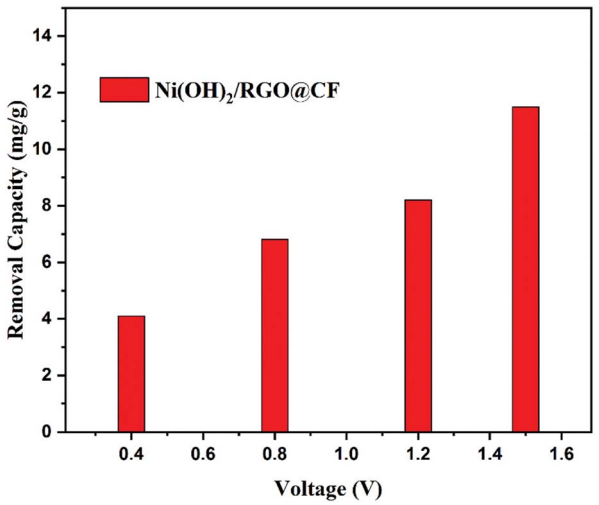

Fig. 6 The CDI performance of $Ni(OH)_2$/RGO@CF nanocomposites.

(R_{ct}) caused by faradaic reactions and the double-layer capacitance that corresponds to the diameters of the semicircle and is related to the conductivity of the material.[32] It can be seen that a smaller diameter of the semicircle was found for $Ni(OH)_2$/RGO@CF, indicating that it offers a faster charge transfer, thus ensuring high capacitive performance. The line in low frequency represents the quick ion diffusion in electrolyte and the adsorption onto the electrode surface, and the nearly vertical line for $Ni(OH)_2$/RGO@CF represents the electrolytes that can be diffused in the host materials facilely. Therefore, the low resistance of $Ni(OH)_2$/RGO@CF is essential for improving the capacitance, which is supported by the simulated equivalent circuit results (Table S1†). Cyclic stability is an important parameter for supercapacitor electrodes. The cycling performances are provided in Fig. 5(b). Due to the combination of graphene, the $Ni(OH)_2$/RGO@CF electrodes showed higher stability compared with pure $Ni(OH)_2$.

In addition, the nanocomposites as potential electrodes for CDI were explored. The CDI performance of $Ni(OH)_2$/RGO@CF was investigated in NaCl solution with various voltage concentrations. Fig. 6 shows the desalination performance of the electrodes at different voltages in the range of 0.4–1.5 V. As calculated, the adsorption amount of NaCl was enhanced with an increase in the potential, and the highest adsorption of $Ni(OH)_2$/RGO@CF reached was 11.5 mg g^{-1} at 1.5 V. Moreover, the performance was better than that of our formerly reported RGO/CF.[33]

4. Conclusion

A high-performance $Ni(OH)_2$ nanoarray on RGO@carbon fabric nanocomposites with hierarchical nanostructures was fabricated by a two-step method. The unique structure provides $Ni(OH)_2$ nanosheets a high conductivity current collector that helps to lower the resistance. Then, the $Ni(OH)_2$ nanoarrays grow further on the collector with a separated structure, which endows a higher electrochemical active site. By employing the above, RGO/$Ni(OH)_2$@carbon fabric nanocomposites delivered a higher capacitance (1325 F g^{-1} at 1 A g^{-1}), and the electrosorption capacity of this electrode was 11.5 mg g^{-1} with an electrical voltage of 1.5 V. This $Ni(OH)_2$/RGO@carbon fabric nanocomposites can be a candidate electrode for efficient CDI process in brackish water desalination and supercapacitor.

Conflicts of interest

There are no conflicts to declare.

Acknowledgements

This work was financially supported by the National Natural Science Foundation of China (21976177) and the National Key Research and Development Program of China (2018YFA0209302).

References

1 P. Simon and Y. Gogotsi, Materials for electrochemical capacitors, *Nat. Mater.*, 2008, **7**, 845–854.
2 H. Wang, Y. Liang, T. Mirfakhrai, Z. Chen, H. S. Casalongue and H. Dai, Advanced asymmetrical supercapacitors based on graphene hybrid materials, *Nano Res.*, 2011, **4**, 729–736.
3 W. Wei, X. Cui, W. Chen and D. G. Ivey, Manganese oxide-based materials as electrochemical supercapacitor electrodes, *Chem. Soc. Rev.*, 2011, **40**, 1697–1721.
4 G. Wang, L. Zhang and J. Zhang, A review of electrode materials for electrochemical supercapacitors, *Chem. Soc. Rev.*, 2012, **41**, 797–828.
5 C. Liu, H. Song, C. Zhang, Y. Liu, C. Zhang, X. Nan and G. Cao, Coherent Mn3O4-carbon nanocomposites with enhanced energy-storage capacitance, *Nano Res.*, 2015, **8**, 3372–3383.
6 J. Chmiola, C. Largeot, P.-L. Taberna, P. Simon and Y. Gogotsi, Monolithic Carbide-Derived Carbon Films for Micro-Supercapacitors, *Science*, 2010, **328**, 480–483.
7 Z. Wang, W. Jia, M. Jiang, C. Chen and Y. Li, Microwave-assisted synthesis of layer-by-layer ultra-large and thin NiAl-LDH/RGO nanocomposites and their excellent performance as electrodes, *Sci. China Mater.*, 2015, **58**, 944–952.
8 P. Chen, H. Chen, J. Qiu and C. Zhou, Inkjet Printing of Single-Walled Carbon Nanotube/RuO_2 Nanowire Supercapacitors on Cloth Fabrics and Flexible Substrates, *Nano Res.*, 2010, **3**, 594–603.
9 L. Peng, X. Peng, B. Liu, C. Wu, Y. Xie and G. Yu, Ultrathin Two-Dimensional MnO_2/Graphene Hybrid Nanostructures for High-Performance, Flexible Planar Supercapacitors, *Nano Lett.*, 2013, **13**, 2151–2157.
10 Z. Wang, C. Ma, H. Wang, Z. Liu and Z. Hao, Facilely synthesized Fe_2O_3-graphene nanocomposite as novel electrode materials for supercapacitors with high performance, *J. Alloys Compd.*, 2013, **552**, 486–491.
11 Z. Wang, X. Zhang, J. Wang, L. Zou, Z. Liu and Z. Hao, Preparation and capacitance properties of graphene/NiAl

layered double-hydroxide nanocomposite, *J. Colloid Interface Sci.*, 2013, **396**, 251–257.

12 S. Cho, M. Kim and J. Jang, Screen-Printable and Flexible RuO_2 Nanoparticle-Decorated PEDOT:PSS/Graphene Nanocomposite with Enhanced Electrical and Electrochemical Performances for High-Capacity Supercapacitor, *ACS Appl. Mater. Interfaces*, 2015, **7**, 10213–10227.

13 T. Sichumsaeng, N. Chanlek and S. Maensiri, Effect of various electrolytes on the electrochemical properties of $Ni(OH)_2$ nanostructures, *Appl. Surf. Sci.*, 2018, **446**, 177–186.

14 E.-C. Cho, C.-W. Chang-Jian, J.-H. Huang, J.-A. Chou, W.-L. Syu, Y.-L. Chen, K.-C. Lee and Y.-S. Hsiao, Phase and morphology control in the synthesis of Co_3O_4 nanosphere/α-$Co(OH)_2$ nanosheet hybrids for application in supercapacitors, *J. Taiwan Inst. Chem. Eng.*, 2020, **110**, 163–172.

15 C. Fang and D. Zhang, A large areal capacitance structural supercapacitor with a 3D rGO@MnO_2 foam electrode and polyacrylic acid–Portland cement–KOH electrolyte, *J. Mater. Chem. A*, 2020, **8**, 12586–12593.

16 T. S. Ghadge, A. L. Jadhav and B. J. Lokhande, Synthesis and electrochemical study of ruthenium influenced copper oxide electrodes prepared by self anodization, *J. Alloys Compd.*, 2020, **824**, 153860.

17 S. Jeon, J. H. Jeong, H. Yoo, H. K. Yu, B.-H. Kim and M. H. Kim, RuO_2 Nanorods on Electrospun Carbon Nanofibers for Supercapacitors, *ACS Appl. Nano Mater.*, 2020, **3**, 3847–3858.

18 S. G. Kim, J. Jun, Y. K. Kim, J. Kim, J. S. Lee and J. Jang, Facile Synthesis of Co_3O_4-Incorporated Multichannel Carbon Nanofibers for Electrochemical Applications, *ACS Appl. Mater. Interfaces*, 2020, **12**, 20613–20622.

19 Y. Tan, C. Yang, W. Qian and C. Teng, Flower-like MnO2 on layered carbon derived from sisal hemp for asymmetric supercapacitor with enhanced energy density, *J. Alloys Compd.*, 2020, **826**, 154133–154141.

20 X. Yuan, Y. Zhang, Y. Yan, B. Wei, K. Qiao, B. Zhu, X. Cai and T.-W. Chou, Tunable synthesis of biomass-based hierarchical porous carbon scaffold@MnO_2 nanohybrids for asymmetric supercapacitor, *Chem. Eng. J.*, 2020, **393**, 1–11.

21 Y. Wang, Z. Shi, Y. Huang, Y. Ma, C. Wang, M. Chen and Y. Chen, Supercapacitor Devices Based on Graphene Materials, *J. Phys. Chem. C*, 2009, **113**, 13103–13107.

22 Z. Wang, X. Zhang, Y. Li, Z. Liu and Z. Hao, Synthesis of graphene-$NiFe_2O_4$ nanocomposites and their electrochemical capacitive behavior, *J. Mater. Chem. A*, 2013, **1**, 6393–6399.

23 Y. W. Zhu, S. Murali, M. D. Stoller, K. J. Ganesh, W. W. Cai, P. J. Ferreira, A. Pirkle, R. M. Wallace, K. A. Cychosz, M. Thommes, D. Su, E. A. Stach and R. S. Ruoff, Carbon-Based Supercapacitors Produced by Activation of Graphene, *Science*, 2011, **332**, 1537–1541.

24 M. Pumera, Graphene-based nanomaterials and their electrochemistry, *Chem. Soc. Rev.*, 2010, **39**, 4146–4157.

25 X. Yang, J. Zhu, L. Qiu and D. Li, Bioinspired Effective Prevention of Restacking in Multilayered Graphene Films: Towards the Next Generation of High-Performance Supercapacitors, *Adv. Mater.*, 2011, **23**, 2833–2838.

26 L. L. Zhang, X. Zhao, M. D. Stoller, Y. Zhu, H. Ji, S. Murali, Y. Wu, S. Perales, B. Clevenger and R. S. Ruoff, Highly Conductive and Porous Activated Reduced Graphene Oxide Films for High-Power Supercapacitors, *Nano Lett.*, 2012, **12**, 1806–1812.

27 Q. Li, H. Ni, Y. Cai, X. Cai, Y. Liu, G. Chen, L.-Z. Fan and Y. Wang, Preparation and supercapacitor application of the single crystal nickel hydroxide and oxide nanosheets, *Mater. Res. Bull.*, 2013, **48**, 3518–3526.

28 K. K. Purushothaman, I. M. Babu, B. Sethuraman and G. Muralidharan, Nanosheet-Assembled NiO Microstructures for High-Performance Supercapacitors, *ACS Appl. Mater. Interfaces*, 2013, **5**, 10767–10773.

29 D. Sun, X. Yan, J. Lang and Q. Xue, High performance supercapacitor electrode based on graphene paper *via* flame-induced reduction of graphene oxide paper, *J. Power Sources*, 2013, **222**, 52–58.

30 M. Shen, L. Ma, J. Zhu, X. Li and C. Wang, An assembled-nanosheets discus-like $Ni(OH)_2$ hierarchical structure as a high performance electrode material for supercapacitors, *RSC Adv.*, 2015, **5**, 59659–59664.

31 M. Huang, Y. Zhang, F. Li, L. Zhang, Z. Wen and Q. Liu, Facile synthesis of hierarchical Co_3O_4@MnO_2 core-shell arrays on Ni foam for asymmetric supercapacitors, *J. Power Sources*, 2014, **252**, 98–106.

32 Z. Lei, L. Lu and X. S. Zhao, The electrocapacitive properties of graphene oxide reduced by urea, *Energy Environ. Sci.*, 2012, **5**, 6391–6399.

33 X. Liu, T. Chen, W. C. Qiao, Z. Wang and L. Yu, Fabrication of graphene/activated carbon nanofiber composites for high performance capacitive deionization, *J. Taiwan Inst. Chem. Eng.*, 2017, **72**, 213–219.

34 D. Ghosh, S. Giri, M. Manda and C. K. Das, High performance supercapacitor electrode material based on vertically aligned PANI grown on reduced graphene oxide/$Ni(OH)_2$ hybrid composite, *RSC Adv.*, 2014, **4**, 26094–26101.

35 H. Wang, Y. Q. Song, W. S. Liu and L. F. Yan, Three dimensional $Ni(OH)_2$/rGO hydrogel as binder-free electrode for asymmetric supercapacitor, *J. Alloys Compd.*, 2018, **735**, 2428–2435.